Research Article Vol. 30, No. 10 / 9 May 2022 / Optics Express 15978
Optics EXPRESS

Tunable high-order Bessel-like beam generation based on cross-phase modulation

JINPENG YUAN,[1,2] XUEWEN WANG,[1,2] LIRONG WANG,[1,2,*] LIANTUAN XIAO,[1,2] AND SUOTANG JIA[1,2]

[1]State Key Laboratory of Quantum Optics and Quantum Optics Devices, Institute of Laser Spectroscopy, Shanxi University, 92 Wucheng Road, Taiyuan 030006, China
[2]Collaborative Innovation Center of Extreme Optics, Shanxi University, 92 Wucheng Road, Taiyuan 030006, China
*wlr@sxu.edu.cn

Abstract: Nonlinear atomic media are promising substitutes for spatial light modulators (SLMs) owing to the high tunability and fast response. We demonstrate the generation of high-order Bessel-like beam based on cross-phase modulation in ^{85}Rb atoms. The atomic medium, whose refractive index is spatially modulated by the focused Gaussian pump beam, acts as a nonlinear focusing lens for the Laguerre-Gaussian probe beam. As a result, the probe beam carries the nonlinear phase shift and is converted into a Bessel-like mode in far-field diffraction. The superior self-healing ability of the generated high-order Bessel-like beam is verified by inserting an obstruction in the beam path, and its high tunability is investigated in terms of the pump beam power and vapor temperature. Furthermore, this novel beam is used in an obstruction-immune rotation sensor to measure the angular velocity. Nonlinear atomic medium as a novel SLM promises considerable application prospects in modulating the light field structure.

1. Introduction

Manipulating the multiple physical dimensions of photons enables a diversity of light-related applications. The spatial structure, beyond the traditional physical dimensions of frequency, time, amplitude, phase, and polarization, has attracted increasing interest. Tailoring the spatial structure of light fields enables the various special light beams, namely structured light in a broad sense [1,2], which have fueled many applications in the fields of optical communications [3], optical sensing [4,5], micromanipulation [6], quantum information processing [7], and super-resolution imaging [8].

Bessel beams [9], containing a central lobe surrounded by a series of concentric rings, have motivated considerable attention for their fascinating non-diffraction and self-healing properties. In particular, high-order Bessel beams carrying orbital angular momentum (OAM) have been widely utilized in material characterization [10], remote sensing [11], optical vortex braiding [12] and particle trapping [13]. The generation of high-order Bessel beam always involves the use of axicon lenses [14,15] and spatial light modulators (SLMs) [11]. However, the output beam of an axicon lens is difficult to adjust due to the fixed cone angle. SLMs have the advantage of high adjustability, but the relatively low damage threshold and slow response limit their application scenarios. Thus, a high-order Bessel beam generation method with high tunability and fast response is required in the optics community.

Recently, various nonlinear media, offering the possibility of manipulating the light field structure through nonlinear effects [16–19], have been proposed as promising substitutes for SLMs. Among the numerous existing nonlinear media, alkali atoms exhibit the novel characteristics of flexible tunability, easy reconfiguration and fast response, which make them powerful tools for generating the structure lights [20–23]. A typical conical emission is generated when a strong beam passes through a nonlinear medium, which is the so-called self-phase modulation

#457232 https://doi.org/10.1364/OE.457232
Journal © 2022 Received 28 Feb 2022; revised 14 Apr 2022; accepted 14 Apr 2022; published 25 Apr 2022

Optics EXPRESS

(SPM) [24,25]. However, as a self-action effect, SPM requires a high input power to generate the nonlinear effect, and introduces stray light due to the serious scattering, which reduces the beam quality. By contrast, cross-action effects [25,26] can achieve the same effect at pump beam powers two orders of magnitude lower, which simultaneously meet the needs of low power and adjustable parameter light sources. To the best of our knowledge, the generation of high-order Bessel beam through the cross-action effect in alkali atoms has not been reported.

In this work, we demonstrate the generation of high-order Bessel-like beam based on the cross-phase modulation (XPM) in ^{85}Rb atoms. The refractive index of the atomic medium is spatially modulated by the Gaussian pump beam. Additionally, the wavefront of the Laguerre-Gaussian (LG) probe beam is reshaped and behaves as a Bessel-like mode in far-field diffraction after it passes through the atomic medium. The intensity distribution and helical phase of the generated beam can be reconstructed when the beam encounters an obstruction in its path. Then, the high tunability of the generated beam is investigated in terms of the pump beam power and vapor temperature. Finally, this novel beam is used in an obstruction-immune rotation sensor to achieve the angular velocity measurement. This work provides an all-optical method for the generation of high-order Bessel beam, which holds substantial potential for manipulating the spatial structure of light fields through nonlinear effects.

2. Method

The schematic of the high-order Bessel-like beam generation is shown in Fig. 1(a). The 780 nm pump and probe beams are provided by a tapered amplifier diode laser (DL TA pro, Toptica). The beam waist is approximately 0.5 mm. The frequency is blue-detuned to the $5S_{1/2}(F = 3) - 5P_{3/2}(F' = 4)$ transition of ^{85}Rb, which is monitored using a wavelength meter (WS-7, High Finesse). The LG probe beam with OAM is generated by a Q-plate, while the Gaussian pump beam is focused through a lens (focal length $f = 300$ mm) to excite the nonlinear effect of atomic medium. The two beams with counter-propagating configuration enter a $10 \times 10 \times 10$ mm^3 vapor cell. The center of the vapor cell is located at the focus of the pump beam, and its temperature is accurately controlled through a self-feedback system. The right side of the vapor cell is taken as the z-axis origin , which is defined as $z = 0$ cm. The intensity profiles

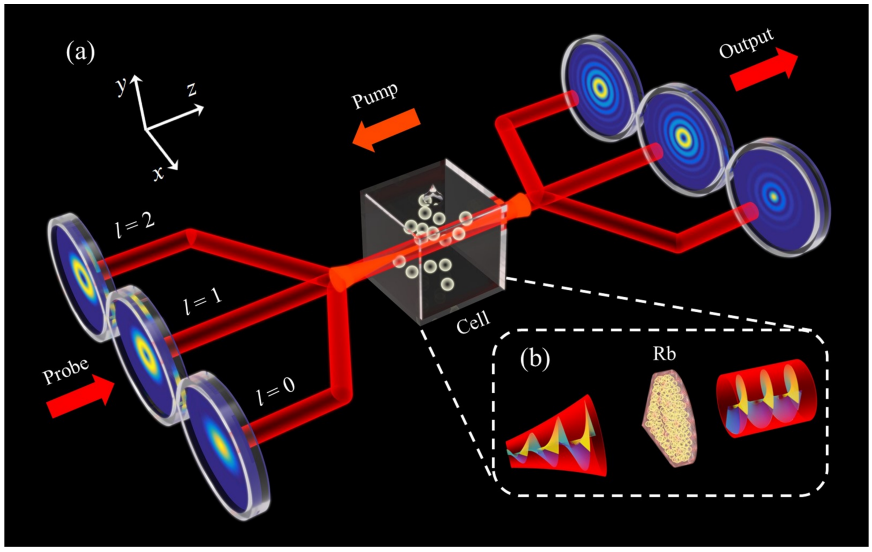

Fig. 1. (a) Schematic and (b) principle of the high-order Bessel-like beam generation.

Optics EXPRESS

of the output probe beam are recorded utilizing a charge-coupled device (CCD). Figure 1(b) depicts the principle of the high-order Bessel-like beam generation. The refractive index of the atomic medium is spatially modulated by the focused Gaussian beam and serves as a nonlinear focused lens, which is equivalent to an axicon lens for the probe beam. The LG beam undergoes a nonlinear phase shift after it passes through the atomic medium, thus converting from a diverging vortex beam into a tightly focused and self-healing high-order Bessel-like beam.

3. Experimental results and discussions

The LG beam, as the input probe beam, introduces a new degree of freedom in the light-related applications owing to the theoretically infinite topological charge, which can be expressed as:

$$E(r,\varphi) = \frac{A}{\omega(\xi)}\left(\frac{\sqrt{2}r}{\omega^2(\xi)}\right)^l L_p^l exp(-il\varphi)exp[ikz - \frac{r^2}{\omega_0^2(1+i\xi)} - i(l+2p+1)\psi_0(\xi)] \tag{1}$$

where k is the wave vector, $r^2 = x^2 + y^2$, φ is the angular coordinate, $\psi_0(\xi) = arctan(\xi)$ is the Gouy phase, L_p^l is the Laguerre polynomial, p is the radial topological charge ($p = 0$ is assumed), l is the topological charge, and A is a constant. The beam waist is ω_0, and $\omega(\xi) = \omega_0(1+\xi^2)^{1/2}$ defines the radius at which the electric field intensity decreases to $e^2/2$ of its maximum value, where $\xi = z/z_R$, in which $z_R = \pi\omega_0^2/\lambda$ is the Rayleigh length. When a strong Gaussian pump beam interacts with the atomic medium, the nonlinear refractive index modulation is induced by the optical Kerr effect, which makes the probe beam carry nonuniform phase shifts in the radial direction on the exit of the vapor cell [27]. Considering that the pump beam is much stronger than the probe beam, we neglect the probe intensity I_1. Then, the phase shift is obtained as [25]:

$$\varphi_{NL} = 2k\int_0^L n_2 I_2(0,0)\frac{\omega_0^2}{\omega^2(\xi)}exp(-\frac{2r^2}{\omega^2(\xi)})dz \tag{2}$$

where L is the length of the sample cell, and $I_2(0,0)$ is the central intensity of the pump beam. Considering that the pump beam at the focus position plays the key role in modulating the phase of the probe beam, Eq. (2) can be approximated as $\varphi_{NL} = 2kn_2LI_2(0,0)exp(-2r^2/\omega_0^2)$. Thus, the far-field distribution pattern of the probe beam can be simulated based on the integral formula of Fresnel-Kirchhoff diffraction:

$$I = |\frac{1}{i\lambda D}|^2|\int_0^\infty\int_0^{2\pi} E(r,\varphi)exp(-ikr\theta\cos\varphi)exp[-i(\frac{kr^2}{2R(z)} + \varphi_{NL})]rdrd\varphi|^2 \tag{3}$$

where D is the distance between the exit of the sample cell and the CCD, $R(z) = z + z_R^2/z$ is the radius of curvature of the wave face of the Gaussian pump beam, θ is the far-field diffraction angle. Clearly, the Eq. (3) contains the l-order Bessel function, which is written as:

$$J_l(kr\theta) = \frac{(-i)^l}{2\pi}\int_0^{2\pi} exp[-i(kr\theta\cos\varphi + l\varphi)]d\varphi \tag{4}$$

Figure 2(a) shows the theoretical simulations with different topological charges, the probe beam carrying the nonlinear phase shift exhibits the typical intensity distributions of the Bessel beam. The experimental results are shown in Fig. 2(b), the intensity distributions of the generated beams are similar to the Bessel-Gaussian beams described by the Bessel function, which are in excellent agreement with the theoretical simulations. Here, the laser frequency is blue-detuned approximately 1 GHz relative to the $5S_{1/2}$ ($F = 3$) - $5P_{3/2}$ ($F' = 4$) transition of ^{85}Rb. The pump and probe beam powers are fixed at 40 and 0.1 mW respectively, and the vapor temperature is set to 140 °C. The atomic vapor with a spatially-varying refractive index due to the modulation of

Optics EXPRESS

the pump beam acts as a nonlinear focusing lens for the probe beam. Thus, the spatial phase distribution of the probe beam is reshaped and the far-field diffraction pattern carrying the nonlinear phase shift is converted into a non-Gaussian mode, which behaves as a Bessel-like beam. The cylindrical lens is used to measure the topological charge of the generated beam by transforming incident photon momentum to position at the focal plane [28], and the corresponding profiles are shown in Fig. 2(c). The cylindrical lens profiles clearly demonstrate the exact order of the generated high-order Bessel-like beam, whose topological charge is the same as that of the input beam.

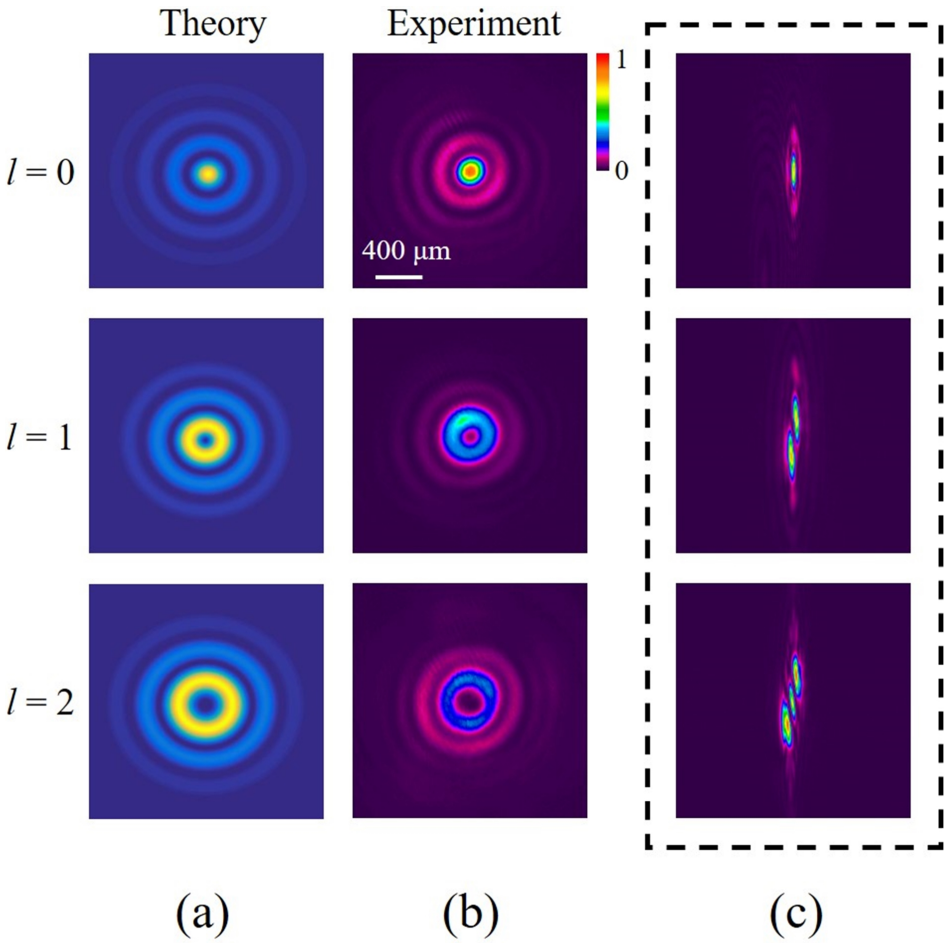

Fig. 2. (a) Simulated and (b) experimental intensity profiles of the high-order Bessel-like beam. (c) Corresponding cylindrical lens profiles of the generated high-order Bessel-like beam.

We further examine the propagation property of the generated high-order Bessel-like beam in the presence of an obstruction. When the obstruction is located in the Bessel region, the generated Bessel-like beam can be reconstructed. Figure 3(a) shows the intensity profiles of the high-order Bessel-like beam at different propagation positions with an obstruction. Here the related experimental parameters are the same as in Fig. 2. The obstruction is a thin quartz plate with a black spot made of printing ink of about 300 μm diameter, which is inserted at z = 30.5 cm. The main lobe of the high-order Bessel-like beam is totally blocked by the obstruction at z = 31 cm and gradually recovers with increasing propagation distance. Finally, the unscreened light

Optics EXPRESS

bypasses the obstruction and reconstructs the intensity profile of the high-order Bessel-like beam at z = 40.9 cm. A cylindrical lens is also used to verify the topological charge in this process, and the corresponding profiles are shown in Fig. 3(b). As expected, both the intensity distribution and helical phase of the output beams are reconstructed when encountering an obstruction in the beam path.

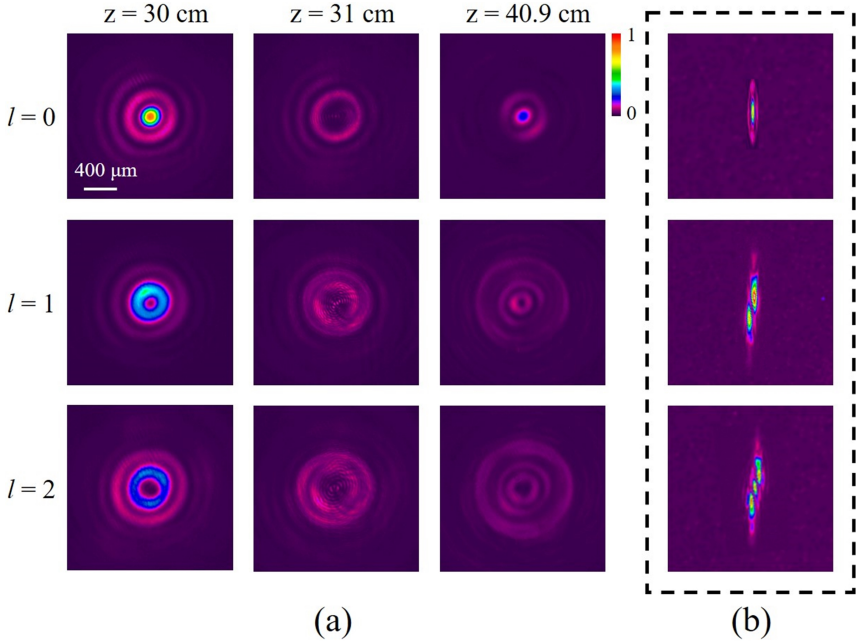

Fig. 3. (a) Intensity profiles of the generated high-order Bessel-like beam at different propagation positions with an obstruction inserted at z = 30.5 cm. (b) Corresponding cylindrical lens profile after the obstruction.

Figures 4(a) and 4(b) show the intensity profile and extracted radius of the main lobe of the generated high-order Bessel-like beam at different pump beam powers with the probe beam power of 0.1 mW and vapor temperature of 140 °C. The radius of the main lobe of generated high-order Bessel-like beam decreases with increasing pump beam power. According to Eq. (2), the nonlinear phase shift φ_{NL} increases as the pump beam power increases, which indicates that the focusing strength is enhanced. The intensity profile and radius of the main lobe of the generated high-order Bessel-like beam as increasing vapor temperature are shown in Figs. 4(c) and (d) respectively, when the pump beam power is fixed at 120 mW. The refractive index n_2 is in proportional to the real part of the third-order nonlinear susceptibility, which is positively correlated with the atomic number density. As the vapor temperature increases, the atomic density increases, and n_2 accordingly becomes larger. The focusing strength is enhanced, and the radius of the main lobe decreases with increasing vapor temperature. Therefore, the beam parameter can be adjusted by varying the pump beam power and vapor temperature. The high tunability of the generated high-order Bessel-like beam is beneficial to its practical application. Furthermore, the output probe beam retains a transmittance higher than 90% owing to the cross-induced transparency.

The generated high-order Bessel-like beam, combining the advantages of the spiral phase and self-healing ability, can be served as a powerful tool in obstruction-immune rotation sensors, which cannot be achieved by the traditional Gaussian and LG beams. The generated high-order Bessel-like beam is coaxially incident into the center of the rotating object, resulting in the

Optics EXPRESS

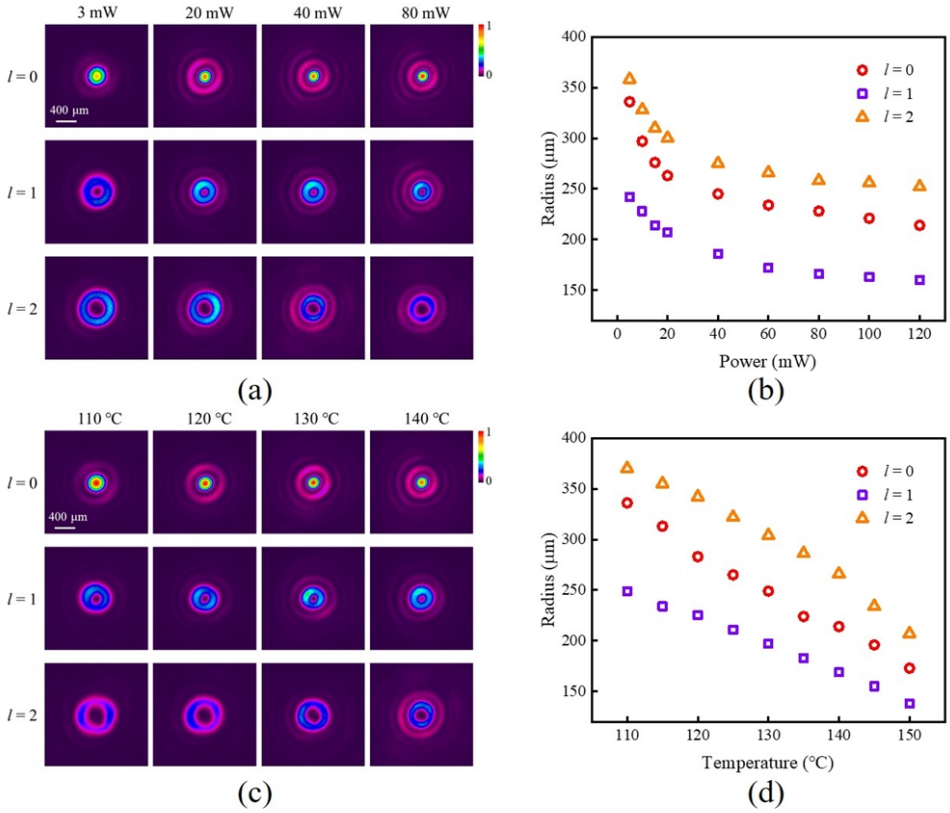

Fig. 4. (a) Intensity profile and (b) radius of the main lobe of the generated high-order Bessel-like beam at different pump beam powers. (c) Intensity profile and (d) radius of the main lobe of the generated high-order Bessel-like beam at different vapor temperatures.

rotational Doppler shift due to the existence of a small angle $\alpha = l\lambda/(2\pi r)$ between the Poyting vector and the axis of rotation, in which r is the radius from the beam axis. The rotational Doppler shift [4,11] is $\Delta f = f_0 v \sin\alpha/c$, where f_0 is the unshifted frequency, and v is the line speed of an arbitrary point in the incident plane. For a small α, the shift can be written as:

$$\Delta f = \frac{f_0 v \sin\alpha}{c} = f_0 \frac{r\Omega}{\lambda f_0} \cdot \frac{l\lambda}{2\pi r} = \frac{l\Omega}{2\pi} \tag{5}$$

here Ω is the angular velocity. The frequency shift is obtained through the beat frequency detection between the beam reflected from the rotating surface and the original Gaussian beam. In the experiment, the rotating object located at $z = 40.9$ cm is a chopper (SR540, Stanford Research Systems) with a precisely modulated frequency $f_{mod} = \Omega/(2\pi)$.

Figure 5(a) shows the rotational Doppler shift with different modulation frequencies and topological charges l. For the same l, the frequency shift increases linearly with the modulation frequency according to the Eq. (5). The inset shows the normalized frequency domain signal with a high signal-to-noise ratio (SNR) when the modulation frequency is 26.66 Hz, and the measured rotational doppler shifts are 26.55 ± 0.21 and 53.34 ± 0.19 Hz for the $l = 1$ and 2, respectively. The measurement error [29] of the frequency domain signal is given by $\delta f = \sqrt{3}/(\sqrt{2}\pi\tau\sqrt{SNR})$, where the cumulative detection time τ is 1 s. In addition, the generated high-order Bessel-like beam can effectively be used to measure the angular velocity in the presence of an obstruction. Figures 5(b) and (c) show the normalized frequency domain signals with the generated Bessel-like

Optics EXPRESS

beam and LG beam for $l = 2$ when the modulation frequency is 26.66 Hz. When there is no obstruction, a clearly distinguishable peak emerges with the same frequency shift of 53.34 Hz using both the two beams. Once the obstruction is placed, the peak intensity for the generated Bessel-like beam decreases a bit but can still be observed obviously. However, for the LG beam, the frequency domain signal is totally mess.

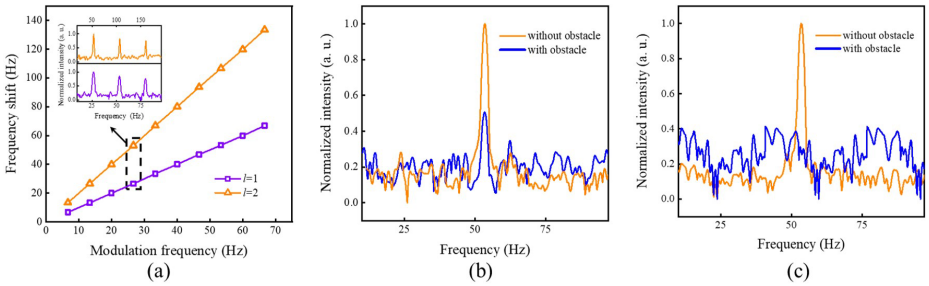

Fig. 5. (a) Rotational Doppler shift for different modulation frequencies and topological charges. The inset shows the normalized frequency domain signal. Normalized frequency domain signal with the (b) high-order Bessel-like beam and (c) LG beam.

4. Conclusions

In summary, we present an all-optical method to generate the high-order Bessel-like beam based on the XPM in ^{85}Rb atoms. The atomic medium modulated by the focused Gaussian beam serves as a nonlinear focused lens, which is equivalent to an axicon lens for the probe beam. The LG probe beam undergoes a nonlinear phase shift after it passes through an atomic medium, thereby converting from a diverging vortex beam into a tightly focused and self-healing high-order Bessel-like beam. Furthermore, the intensity distribution and helical phase of the generated high-order Bessel-like beam can be reconstructed when encountering an obstruction on the beam path. The beam parameter can be flexibly adjusted by varying the pump beam power and vapor temperature. Furthermore, this novel beam can be serves as a powerful tool in obstruction-immune rotation sensors to measure the angular velocity. This work holds tremendous promises for manipulating the spatial structure of light field through the nonlinear effect.

Funding. National Natural Science Foundation of China (61875112, 62075121); Program for Sanjin Scholars of Shanxi Province; Key Research and Development Program of Shanxi Province for International Cooperation (201803D421034); Shanxi "1331 Project".

Disclosures. The authors declare no conflicts of interest.

Data availability. Data underlying the results presented in this paper are not publicly available at this time but may be obtained from the authors upon reasonable request.

References

1. A. Forbes, M. D. Oliveira, and M. R. Dennis, "Structured light," Nat. Photonics **15**(4), 253–262 (2021).
2. Y. Bai, H. Lv, X. Fu, and Y. Yang, "Vortex beam: generation and detection of orbital angular momentum," Chin. Opt. Lett. **20**(1), 012601 (2022).
3. J. Yuan, H. Zhang, C. Wu, L. Wang, L. Xiao, and S. Jia, "Tunable optical vortex array in a two-dimensional electromagnetically induced atomic lattice," Opt. Lett. **46**(17), 4184–4187 (2021).
4. M. P. J. Lavery, F. C. Speirits, S. M. Barnett, and M. J. Padgett, "Detection of a spinning object using light's orbital angular momentum," Science **341**(6145), 537–540 (2013).
5. P. Jia, Z. Li, Y. Hu, Z. Chen, and J. Xu, "Visualizing a nonlinear response in a Schrödinger wave," Phys. Rev. Lett. **123**(23), 234101 (2019).
6. J. Chen, J. Ng, Z. Lin, and C. T. Chan, "Optical pulling force," Nat. Photonics **5**(9), 531–534 (2011).
7. Y. Zhang, M. Agnew, T. Roger, F. S. Roux, T. Konrad, D. Faccio, J. Leach, and A. Forbes, "Simultaneous entanglement swapping of multiple orbital angular momentum states of light," Nat. Commun. **8**(1), 632 (2017).

Optics EXPRESS

8. F. O. Fahrbach, P. Simon, and A. Rohrbach, "Microscopy with self-reconstructing beams," Nat. Photonics **4**(11), 780–785 (2010).
9. J. Durnin, J. J. Miceli, and J. H. Eberly, "Diffraction-free beams," Phys. Rev. Lett. **58**(15), 1499–1501 (1987).
10. A. H. Dorrah, M. Zamboni-Rached, and M. Mojahedi, "Experimental demonstration of tunable refractometer based on orbital angular momentum of longitudinally structured light," Light: Sci. Appl. **7**(1), 40 (2018).
11. S. Fu, T. Wang, Z. Zhang, Y. Zhai, and C. Gao, "Non-diffractive bessel-gauss beams for the detection of rotating object free of obstructions," Opt. Express **25**(17), 20098–20108 (2017).
12. A. A. Voitiv, J. M. Andersen, M. E. Siemens, and M. T. Lusk, "Optical vortex braiding with bessel beams," Opt. Lett. **45**(6), 1321–1324 (2020).
13. H. Wang, J. Wang, W. Dong, Y. Han, L. A. Ambrosio, and L. Liu, "Theoretical prediction of photophoretic force on a dielectric sphere illuminated by a circularly symmetric high-order bessel beam: on-axis case," Opt. Express **29**(17), 26894 (2021).
14. J. Arlt and K. Dholakia, "Generation of high-order bessel beams by use of an axicon," Opt. Commun. **177**(1-6), 297–301 (2000).
15. Y. Arita, J. Lee, H. Kawaguchi, R. Matsuo, K. Miyamoto, K. Dholakia, and T. Omatsu, "Photopolymerization with high-order bessel light beams," Opt. Lett. **45**(14), 4080–4083 (2020).
16. W. R. Callen, B. G. Huth, and R. H. Pantell, "Optical patterns of thermally self-defocused light," Appl. Phys. Lett. **11**(3), 103–105 (1967).
17. Q. Zhang, X. Cheng, H. Chen, B. He, Z. Ren, Y. Zhang, and J. Bai, "Diffraction-free, self-reconstructing bessel beam generation using thermal nonlinear optical effect," Appl. Phys. Lett. **111**(16), 161103 (2017).
18. Q. Zhang, X. Cheng, H. Chen, B. He, Z. Ren, Y. Zhang, and J. Bai, "Enhancement of phase conjugation degenerate four-wave mixing using a Bessel beam," Photonics Res. **6**(3), 162–167 (2018).
19. L. Cheng, Z. Zhang, L. Zhang, D. Ma, G. Yang, T. Dong, and Y. Zhang, "Manipulation of a ring-shaped beam via spatial self- and cross-phase modulation at lower intensity," Phys. Chem. Chem. Phys. **21**(14), 7618–7622 (2019).
20. Z. Zhang, R. Wang, Y. Zhang, Y. V. Kartashov, F. Li, H. Zhong, H. Guan, K. Gao, F. Li, Y. Zhang, and M. Xiao, "Observation of edge solitons in photonic graphene," Nat. Commun. **11**(1), 1902 (2020).
21. Y. Liao, C. Song, Y. Xiang, and X. Dai, "Recent advances in spatial self-phase modulation with 2d materials and its applications," Ann. Phys. **532**(12), 2000322 (2020).
22. Y. Zhang, X. Cheng, X. Yin, J. Bai, P. Zhao, and Z. Ren, "Research of far-field diffraction intensity pattern in hot atomic Rb sample," Opt. Express **23**(5), 5468–5476 (2015).
23. H. Hu, D. Luo, C. Pan, Y. Qin, Y. Zhang, D. Wei, H. Chen, H. Gao, and F. Li, "Collapse of hybrid vector beam in Rb atomic vapor," Opt. Lett. **46**(11), 2614–2617 (2021).
24. J. D. Swaim, K. N. David, E. M. Knutson, C. Rios, O. Danaci, and R. T. Glasser, "Atomic vapor as a source of tunable, non-gaussian self-reconstructing optical modes," Sci. Rep. **7**(1), 42311 (2017).
25. X. Cheng, Q. Zhang, H. Chen, B. He, Z. Ren, Y. Zhang, and J. Bai, "Demonstration of bessel-like beam with variable parameters generated using cross-phase modulation," Opt. Express **25**(21), 25257–25266 (2017).
26. Q. Zhang, X. Cheng, B. He, H. Chen, Z. Ren, and J. Bai, "Size-variable dark-hollow beam generation using cross-phase modulation," Opt. Laser Technol. **119**, 105582 (2019).
27. S. Wang, J. Yuan, L. Wang, L. Xiao, and S. Jia, "Measurement of the kerr nonlinear refractive index of the rb vapor based on an optical frequency comb using the z-scan method," Opt. Express **28**(25), 38334–38342 (2020).
28. S. N. Alperin, R. D. Niederriter, J. T. Gopinath, and M. E. Siemens, "Quantitative measurement of the orbital angular momentum of light with a single, stationary lens," Opt. Lett. **41**(21), 5019–5022 (2016).
29. Z. Zhang, L. Cen, F. Wang, and Y. Zhao, "Tiny velocity measurement using rotating petal-like mode of orbital angular momentum," Opt. Lett. **46**(19), 4805–4808 (2021).